NATIONAL AND KAPODISTRIAN UNIVERSITY OF ATHENS

SCHOOL OF SCIENCE
DEPARTMENT OF INFORMATICS AND TELECOMMUNICATION

MSc THESIS

Exploration of 3D structured artificial materials using additive manufacturing for microwave applications

Pablo Helio Zapata Cano

Supervisors: **Erika Vandelle (Thales Research and Technology),**
Dimitris Syvridis (University of Athens)

PARIS

August 2021

ΕΘΝΙΚΟ ΚΑΙ ΚΑΠΟΔΙΣΤΡΙΑΚΟ ΠΑΝΕΠΙΣΤΗΜΙΟ ΑΘΗΝΩΝ

ΣΧΟΛΗ ΘΕΤΙΚΩΝ ΕΠΙΣΤΗΜΩΝ
ΤΜΗΜΑ ΠΛΗΡΟΦΟΡΙΚΗΣ ΚΑΙ ΤΗΛΕΠΙΚΟΙΝΩΝΙΩΝ

ΔΙΠΛΩΜΑΤΙΚΗ ΕΡΓΑΣΙΑ

Διερεύνηση τρισδιάστατων δομημένων τεχνητών υλικών με χρήση προσθετικής κατασκευής για εφαρμογές μικροκυμάτων

Pablo Helio Zapata Cano

Επιβλέποντες: **Erika Vandelle (Thales Research and Technology),
Dimitris Syvridis (University of Athens)**

ΠΑΡΙΣΙ

ΑΥΓΟΥΣΤΟΣ 2021

MSc THESIS

Exploration of 3D structured artificial materials using additive manufacturing for microwave applications

Pablo Helio Zapata Cano
S.N.: 207853771677

SUPERVISOR: **Erika Vandelle (Thales Research and Technology),**
Dimitris Syvridis (University of Athens)

ΔΙΠΛΩΜΑΤΙΚΗ ΕΡΓΑΣΙΑ

Διερεύνηση τρισδιάστατων δομημένων τεχνητών υλικών με χρήση προσθετικής κατασκευής για εφαρμογές μικροκυμάτων

Pablo Helio Zapata Cano
Α.Μ.: 207853771677

ΕΠΙΒΛΕΠΟΝΤΕΣ: **Erika Vandelle (Thales Research and Technology),**
Dimitris Syvridis (University of Athens)

ABSTRACT

This master thesis consists of the exploration of periodic structures, compatible with additive manufacturing fabrication techniques and complex synthesized materials, and their application in the design of microwave absorbers. Two different methodologies are proposed with the aim of controlling the absorption level over a large range of frequencies (2-20 GHz). The first one consists of the study of the resonant phenomena of lossy dielectric resonators with dispersive material properties, whereas the second one relies on evolutionary optimization techniques to design multi-material structures. Finally, a prototype is designed, fabricated, and characterized. This demonstrator is obtained from the combination of two commercial materials and provides an absorption level above 90% over the 2-12 GHz frequency band for the TM polarization.

SUBJECT AREA: Microwave engineering, applied electromagnetics.

KEYWORDS: Microwave absorber, 3-D printing, periodic structures, engineered materials.

ΠΕΡΙΛΗΨΗ

Η παρούσα μεταπτυχιακή διατριβή συνίσταται στη διερεύνηση περιοδικών δομών, συμβατών με τεχνικές κατασκευής προσθετικής κατασκευής και σύνθετα συνθετικά υλικά, και στην εφαρμογή τους στο σχεδιασμό απορροφητών μικροκυμάτων. Προτείνονται δύο διαφορετικές μεθοδολογίες με στόχο τον έλεγχο του επιπέδου απορρόφησης σε ένα μεγάλο εύρος συχνοτήτων (2-20 GHz). Η πρώτη συνίσταται στη μελέτη των φαινομένων συντονισμού απωλεστικών διηλεκτρικών αντηχείων με ιδιότητες υλικών διασποράς, ενώ η δεύτερη βασίζεται σε τεχνικές εξελικτικής βελτιστοποίησης για τον σχεδιασμό δομών πολλαπλών υλικών. Τέλος, σχεδιάζεται, κατασκευάζεται και χαρακτηρίζεται ένα πρωτότυπο. Αυτός ο επιδεικτικός εξοπλισμός προκύπτει από το συνδυασμό δύο εμπορικών υλικών και παρέχει επίπεδο απορρόφησης άνω του 90% στη ζώνη συχνοτήτων 2-12 GHz για την πόλωση TM.

CONTENTS

LIST OF FIGURES

LIST OF TABLES

PREFACE

1. INTRODUCTION

This work states the finalisation of my studies under the Smart Telecom and Sensing Networks (SMARTNET) Erasmus Mundus Joint Master Degree (EMJMD) programme at Institute Polytechnique de Paris (IP Paris) and University of Athens (UoA). This master's thesis is the result of a six-months internship at Thales Research & Technology (TRT) on the topic "Exploration of 3D structured artificial materials using additive manufacturing for microwave applications".

Thales is a French company whose activity is divided into 5 main areas: Aerospace, Space, Defence, Security and Transportation. TRT constitutes the research section, and collaborates with the rest of Thales divisions. This work is carried out within the Laboratory of Components and Technological Demonstrators (LCDT, from French "Laboratoire de Composants et Démonstrateurs Technologiques"), which is a part of the Technology and Characterisation Research Group (GRTM, from French "Groupe de Recherche Technologies et Mesures"). Its main activities include microwave engineering, antennas, photonics, and microelectromechanical systems (MEMs).

1.1 Motivation

Recently, ambitious target specifications have been set for radio-frequency devices operating in the microwave range (1-100 GHz). These include achieving a robust performance over a large bandwidth for large incident angles and multiple polarizations. Among the functionalities of such devices, the absorption and/or filtering of waves is necessary for a large number of applications. Microwave absorbers are used nowadays, for example, as isolator in anechoic chambers, enabling the testing and characterization of antennas and other radio-frequency devices. Another application of this kind of devices is found in the integration of a (communication) system. In such an environment, metallic components might produce wave reflection and thus interference, and absorbers constitute a practical solution to avoid this phenomenon. Microwave absorbers are also used on stealth applications, with the function of "hiding" some object from a scanning device.

This master thesis consist on the study of several architectures / design techniques for the conception of absorbing devices in the microwave range.

Pablo H. Zapata Cano

1.2 Objectives of the internship

The main objectives of this master thesis can be synthesized as follows:

- Perform a deep study on resonating structures, using electromagnetic theory in addition to full wave simulation to understand the relations between the resonating mode distribution, frequency and resonator geometry.

- Delve deep into periodic structures, with an emphasis on the ones formed by the arrangement of 3-D resonators, and their applications for wave absorption / manipulation.

- Review the recent progress on artificial materials, focusing on 3-D printable composite and their applications for the design of microwave absorbers.

- Define some guidelines / methodology for the design of broadband microwave absorbers playing both with the geometry and the material of the structure to control the level of absorption.

- Gain expertise in the simulation and modeling of periodic structures, both through analytical / numerical methods and full-wave simulation.

- Become familiar with different material characterization techniques and methodologies, and conduct some practical experiments in the laboratory.

- Perform some characterization measurements to evaluate the performance of an absorber at normal and oblique incidence. This includes the familiarization with the set up and equipment, the protocol of the measurement and the post-processing and interpretation of the obtained results.

- Develop some synthesis and critical analysis competences that allows to correctly interpret the obtained results and build reports where the most determining information is highlighted.

1.3 Outline

This document is structured as follows: First, Chapter 2 introduces some theoretical concepts that will be necessary to analyse the structures proposed in this work. Then, Chapter 3 is devoted to provide a definition of microwave absorption, as well as to contextualize this work in the state of the art of the literature. The main software and hardware tools and procedures used for this work are presented in Chapter 4. Next, Chapter 5 presents two methods of design of broadband microwave absorbers with controlled absorption levels using periodic structures. Using some of these principles, a demonstrator has been designed, manufactured and characterized. The results associated to this part are presented in Chapter 6. Finally, Chapter 7 contains some conclusions and final remarks, as well as some ideas for future research lines.

2. MOTIVATION, BACKGROUND

This chapter is devoted to provide the theoretical base necessary for the analysis of the structures studied in this work. Thus, an overview of the interaction of electromagnetic waves with an interface is given, starting from Maxwell equations and reflection/transmission principles and converging into the particular case of periodic structures made of resonators.

2.1 Reflection and transmission of electromagnetic waves

In order to model and analyse the structures investigated in this work, the basic reflection and transmission principles of electromagnetic waves in a material interface should be understood. We start by considering uniform plane waves incident normally on material interfaces. The electric and magnetic fields of a wave propagating along the z-direction in a lossless, homogeneous, and isotropic dielectric are given by the Equation 2.1. The electric field is considered to be linearly polarized in the x-direction, which implies $\mathbf{E}(z) = \hat{\mathbf{x}}E_x = \hat{\mathbf{x}}E(z)$ and $\mathbf{H}(z) = \hat{\mathbf{y}}H_y(z) = \hat{\mathbf{y}}H(z)$.

$$\begin{aligned} E(z) &= E_{0+}e^{-jkz} + E_{0-}e^{jkz} = E_+(z) + E_(z) \\ H(z) &= \frac{1}{\eta}[E_{0+}e^{-jkz} - E_{0-}e^{jkz}] = \frac{1}{\eta}[E_+(z) - E_-(z)] \end{aligned} \tag{2.1}$$

E_+ and E_- (H_+ and H_-) are the forward and backward electric (magnetic) fields. Two useful quantities in interface problems are the wave impedance (Z) and reflection coefficient (Γ), defined as:

$$Z(z) = \frac{E(z)}{H(z)} \qquad \Gamma(z) = \frac{E_-(z)}{E_+(z)} \tag{2.2}$$

For plane waves, the wave impedance is equal to the intrinsic impedance of the medium η, that depends exclusively on the material parameters of the medium. Having η as the intrinsic impedance of the incident medium, and η' as the one of the transmitted medium, one can stablish the following relationships

$$\eta' = \eta\frac{1+\Gamma(z)}{1-\Gamma(z)} \qquad \Gamma(z) = \frac{\eta'-\eta}{\eta'+\eta} \tag{2.3}$$

Moreover, for some structures, it results particularly useful to calculate the impedance by applying transmission line theory. In this case, the expression of the impedance is given by the input impedance Z_{in} of a transmission line as

$$Z_{in}(z) = \eta\frac{\eta' + j\eta\,\mathsf{tanh}(kz)}{\eta + j\eta'\,\mathsf{tanh}(kz)} \tag{2.4}$$

Pablo H. Zapata Cano

In the case of oblique incidence, we differentiate between Transversal Magnetic (TM, horizontal) and Transversal Electric (TE, vertical) polarizations. As depicted in Figure 2.1, in the case of TM polarization, the electric fields lie on the plane of incidence and transverse to the z-direction, whereas in TE polarization, the electric fields are perpendicular to the plane of incidence and transverse to the z-direction.

(a) TM, horizontal, parallel polarization.   *(b) TE, vertical, perpendicular polarization.*
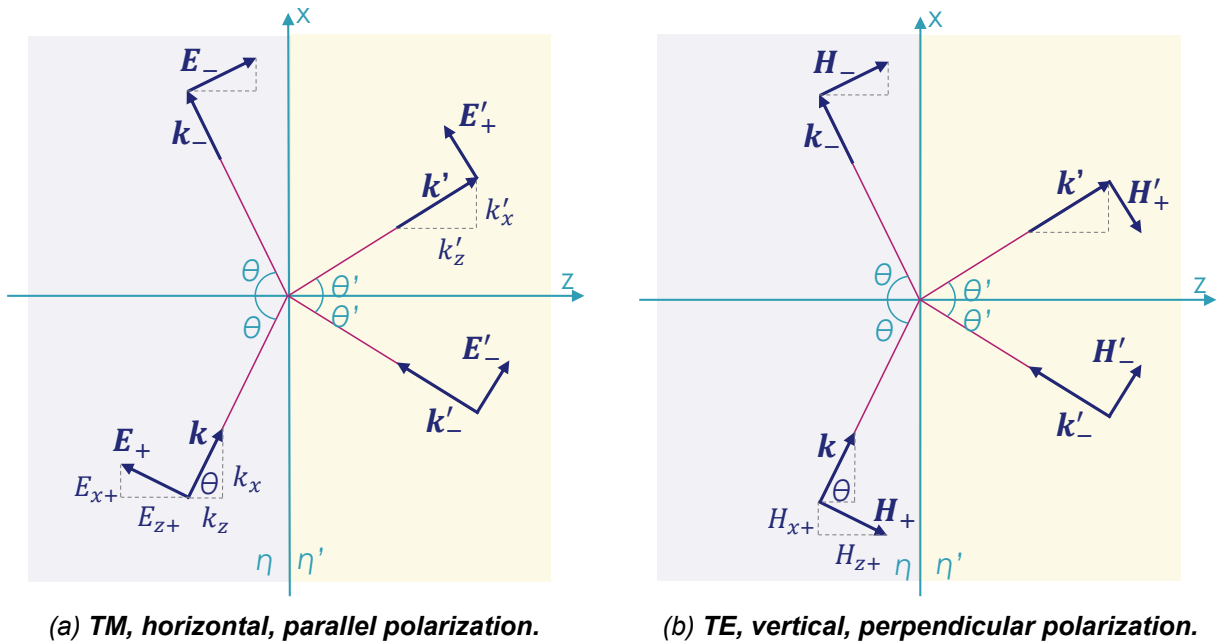
Figure 2.1: *Oblique incidence for TM- and TE- polarized waves.*

Applying Snel's law of refraction and some maths, the transverse fields on the left side of the schematic can be expressed as:

$$\begin{aligned} \mathbf{E}_T(z) &= \hat{\mathbf{x}}E_{TM}(z) + \hat{\mathbf{y}}E_{TE}(z) \\ \mathbf{H}_T(z) &= \hat{\mathbf{y}}H_{TM}(z) - \hat{\mathbf{x}}H_{TE}(z) \end{aligned} \tag{2.5}$$

Using the transverse impedance and summarizing both polarizations in a compact form, where E_T (H_T) stands either for E_{TM} or E_{TE} (H_{TM} or H_{TE}), we obtain:

$$\begin{aligned} E_T(z) &= E_{T+}e^{-jk_zz} + E_{T-}e^{jk_zz} \\ H_T(z) &= \frac{1}{\eta_T}[E_{T+}e^{-jk_zz} - E_{T-}e^{jk_zz}] \end{aligned} \tag{2.6}$$

where the transverse impedance η_T is defined for TM and TE polarizations as:

$$\eta_T = \begin{cases} \eta\cos(\theta), & \text{TM (horizontal) polarization} \\ \frac{\eta}{\cos(\theta)}, & \text{TE (vertical) polarization} \end{cases} \tag{2.7}$$

Similar equations can be found for the right side of the interface [1].

2.2 Electromagnetic waves in periodic structures

Before delving into periodic structures, it is worthwhile to briefly introduce the theoretical basis that describe all (classical) electromagnetic phenomena: Maxwell's equations.

$$\begin{aligned}
\nabla \times \mathbf{E} &= -\frac{\partial \mathbf{B}}{\partial t} \\
\nabla \times \mathbf{H} &= \mathbf{J} + \frac{\partial \mathbf{D}}{\partial t} \\
\nabla \bullet \mathbf{D} &= \rho \\
\nabla \bullet \mathbf{B} &= 0
\end{aligned} \tag{2.8}$$

The first is Faraday's law of induction, the second is Ampère's law, whereas the two last correspond to the Gauss' laws for the electric and magnetic fields. The quantities $\mathbf{E}$ and $\mathbf{H}$ are the electric and magnetic field intensities, measured in V/m and A/m, respectively. $\mathbf{D}$ (C/m^2) refers to the electric flux density (or electric displacement), and $\mathbf{B}$ (W/m^2) to the magnetic flux density (or magnetic induction), whereas ρ (C/m^3) and $\mathbf{J}$ (A/m^2) stand for the volume charge density and electric current density of any external charges.

Periodic structures can be defined as an assembly of identical elements arranged in a one(multiple)-dimension(s) infinite array. When this periodic array is excited by an incident plane wave, we talk about passive arrays. In this case, the incident plane wave will be partly transmitted through the surface and partly reflected by it. In order to properly analyse the interaction of electromagnetic waves and periodic structures, some considerations should be made first. Among them, it is crucial to determine the scale at which periodicity occurs.
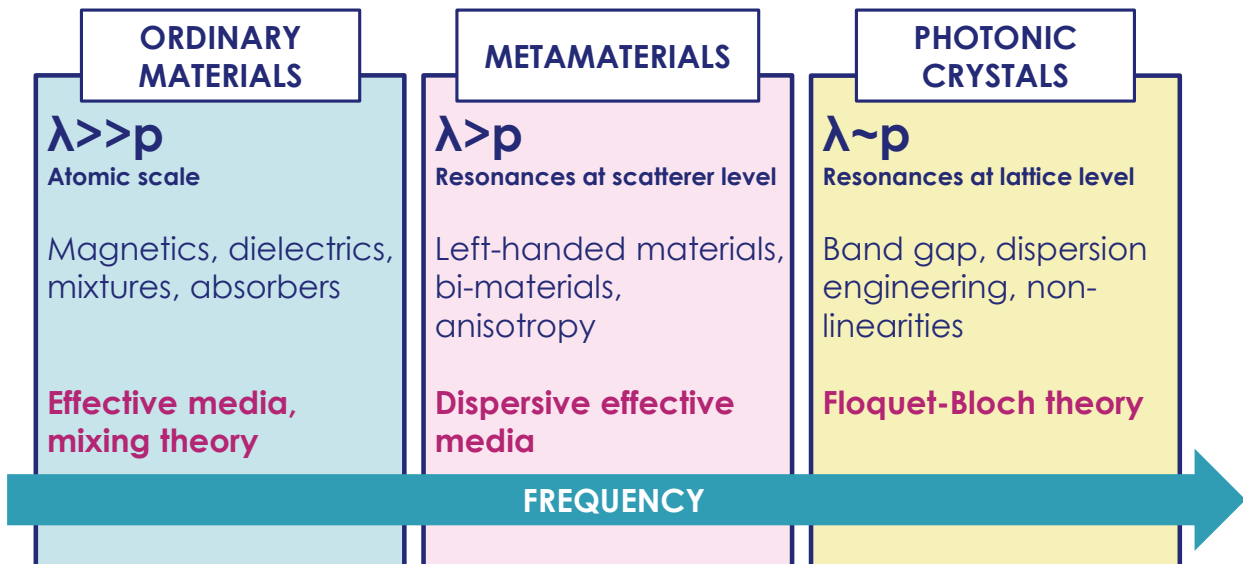

*Figure 2.2: **Characteristic regions of a periodic composite material.***

For instance, periodic structures at the atomic scale form crystal lattices, and they are analysed under the laws of solid state physics, which leads us to talk about "solid state

Pablo H. Zapata Cano

electromagnetics". In this work we will mainly deal with structures that present a periodicity in a much larger scale. However, at microwave frequencies and depending on the dimensions of the structure, it might be still seen as a sub-wavelength composite. A classification with three different characteristic regions, attending to the ratio between the period of the structure and the wavelength, is proposed in Figure 2.2. This will allow us to differentiate bulk materials from dispersive materials, photonic crystals or metamaterials, as well as to delimit the theoretical tool-kits needed to analyse each one of them.

2.2.1 Ordinary materials

The lowest frequency region corresponds to the quasi-static region, in which material and effective medium properties can be determined using classical mixing formulas and theory. Conductors like graphene or gold, dielectrics like teflon or FR4, magnetics such as iron or nickel, and absorbers like salt water or graphite are some of examples of materials within this category. Combination of such ordinary materials, known as mixtures, also form part of this group. Recently, a wide range of nanomaterials with promising performances in the microwave range has been developed. Among them, we find carbons, oxides, sulfides, phosphides, polymers or metals/alloys.

In order to examine the interaction of electromagnetic fields and materials, we need to add to the Maxwell's equations (Equations 2.8) the so-called constitutive relations, that relate the electric and magnetic flux densities **D**, **B** to the field intensities **E** and **H**:

$$\mathbf{D} = \varepsilon\mathbf{E} \qquad \mathbf{B} = \mu\mathbf{H} \qquad \mathbf{J} = \sigma\mathbf{E} \tag{2.9}$$

They depend on the material in which the fields exist, which is described by its fundamental parameters ε, μ and σ (permittivity, permeability and conductivity). The permittivity $\varepsilon = \varepsilon_r \varepsilon_0$ (F/m) is a measure of how well a medium stores electric energy, whereas the permeability $\mu = \mu_r \mu_0$ (H/m) indicates how well a medium stores magnetic energy. ε_0 and μ_0 are the vacuum permittivity and permeability, while ε_r and μ_r are defined as the relative permittivity (or dielectric constant) and permeability. The characteristic impedance η can be expressed in terms of the vacuum impedance $\eta_0 = \sqrt{\mu_0/\varepsilon_0}$ and the material permittivity and permeability as

$$\eta = \eta_0 \sqrt{\frac{\mu_r}{\varepsilon_r}} \tag{2.10}$$

The conductivity σ (1/$\Omega\cdot$ m) describes the degree to which a material conducts electricity. If we classify materials by their conductivity, we find three main groups: insulators, that oppose current ($\sigma \ll 1$, most dielectrics belong to this group); conductors, that easily conduct current ($\sigma \gg 1$, like most metals); and semiconductors, known to have interesting applications due to their tunable conductivity.

If we substitute the constitutive relations (Equations 2.9) into Ampère's law (Equations 2.8)

in the phasor domain, we obtain

$$\nabla \times \mathbf{H} = \sigma \mathbf{E} + jw\varepsilon \mathbf{E} \tag{2.11}$$

Interestingly, the total current is the sum of a real-valued conduction current and an imaginary-valued displacement current. Using the angle δ defined by both real and imaginary vectors, we have

$$\tan \delta_\varepsilon = \frac{\sigma}{w\varepsilon} = \frac{\varepsilon''}{\varepsilon'} \tag{2.12}$$

where the quantity $\tan \delta_\varepsilon$ depicts the dielectric loss tangent, that quantifies the effect of loss on the electromagnetic field within a material. Thus, it is zero for a lossless ($\sigma = 0$) material, and it increases with increasing loss. However, the expression on the left part of Equation 2.12 presumes only ohmic (conduction) loss. The loss tangent can be equivalently calculated by means of the real and imaginary part of the permittivity (right side of Equation 2.12), where no distinction is made between ohmic loss and losses caused by a delayed response of **D** to changing **E**. An analogue reasoning can be made for magnetic losses, obtaining that the magnetic loss tangent is given by $\tan \delta_\mu = \mu''/\mu'$.

2.2.2 Metamaterials

When the period approaches the wavelength (until reaching values around $\lambda/10$), the scatterers forming the periodic structure might resonate themselves. Metamaterials and metasurfaces (two-dimensional arrangement of scatterers) belong to this region. However, electromagnetic metamaterials in which nothing resonates or scatters from unit cells are also realizable within this group. When these conditions are fulfilled, effective medium theory can be applied to extract the effective electromagnetic permittivity and permeability. In that case, the characteristic impedance of (complex, multimaterial) structures can be calculated from the scattering parameters by applying effective medium theory [2].

Metamaterials are famous for presenting some properties that are not attainable with ordinary materials. These "magical" properties are derived from their physical structure, and not form their chemical composition. For example, artificial electrical [3] and/or magnetic [4] responses analogue to the ones of some ordinary materials can be achieved by a suitable structure design. This gives multiple extra degrees of freedom, since geometrical parameters are easier to tune than chemical ones. In this way, simply tuning some geometrical parameters of the unit cell would allow to shift the resonance of the metamaterial, thus changing its effective electromagnetic response. The same principle can be applied to create "non-physical" responses, as in the case of negative parameter metamaterials. Double-negative metamaterials are a recognized example of this practice. They are characterized by having a negative permittivity and permeability, and a negative refractive index, which can lead to some interesting phenomena like negative refraction.

Pablo H. Zapata Cano

2.2.3   Photonic Crystals. Bloch-Floquet theory

When the wavelength becomes comparable to or smaller than the period of the composite, the structure is no longer seen as an effective medium, and the field inside the structure takes on the same symmetry and periodicity of the structure. In this case, the Floquet-Bloch theory can be applied. If we substitute the constitutive relations (Equation 2.9) into the Faraday's and Ampère's laws (Equations in 2.8), we get

$$\nabla \times \mathbf{E} = jw\mu\mathbf{H} \qquad \nabla \times \mathbf{H} = \varepsilon\mathbf{E} \tag{2.13}$$

These are known as the Maxwell's curl equations. Combining source-free Faraday's and Ampère's laws at a fixed frequency ω, the following wave equation is obtained for the magnetic field $\mathbf{H}$:

$$\nabla \times \frac{1}{\varepsilon_r}\nabla \times \mathbf{H} = \left(\frac{w}{c}\right)^2 \mathbf{H} \tag{2.14}$$

Floquet's theorem, due to Gaston Floquet (1883), gives a canonical form for each fundamental matrix solution of a periodic linear system. The study of wave propagation in three-dimensionally periodic media was first developed by Felix Bloch in the 20s. Applying Floquet's mathematics, Bloch proved that waves in such a medium can propagate without scattering, with their behaviour being governed by a periodic envelope function multiplied by a plane wave:

$$\mathbf{E}(\mathbf{r}) = \mathbf{A}(\mathbf{r})e^{j\boldsymbol{\beta}\bullet\mathbf{r}} \tag{2.15}$$

The overall field $\mathbf{E}(\mathbf{r})$ is the combination of the envelope $\mathbf{A}$ and the plane wave term, where β is the Bloch wave vector. If a structure is periodic, then its material properties repeat. This is expressed in terms of lattice vectors as

$$\varepsilon(\mathbf{r}) = \varepsilon(\mathbf{r} + \mathbf{t}_i) \qquad A(\mathbf{r}) = A(\mathbf{r} + \mathbf{t}_i) \tag{2.16}$$

where t_i represents some primitive lattice vectors ($i = 1, 2, 3$ for a three-dimensional periodic crystal). If Equation 2.16 holds, then the Bloch theorem can be applied and the solutions to Equation 2.14 can be chosen of the form

$$\mathbf{H}(\mathbf{r}) = \mathbf{H}_{n,\mathbf{k}}(\mathbf{r})e^{j\mathbf{k}\bullet\mathbf{r}} \tag{2.17}$$

with eigenvalues $\omega_n(\mathbf{k})$, being $\mathbf{H}_{n,\mathbf{k}}(\mathbf{r})$ a periodic envelope satisfying the wave equation

$$(\nabla + j\mathbf{k}) \times \frac{1}{\varepsilon_r}(\nabla + j\mathbf{k}) \times \mathbf{H} = \left(\frac{\omega_n(\mathbf{k})}{c}\right)^2 \mathbf{H}_{n,\mathbf{k}} \tag{2.18}$$

This yields to an eigen-value problem whose solutions are called Bloch modes. They are discrete and orthogonal solutions, which implies that electromagnetic fields in periodic structures can only exist as integer combinations of the Bloch modes of the lattice.

The number of existing propagating Bloch modes is correlated to coefficient ratio between the period of the structure (p) and the wavelength (λ). When p/λ starts approaching 1, diffracted modes start to appear. The number and direction of diffraction orders $\theta(m)$ vary according to p/λ, the incident angle θ_{inc}, and the incident and transmission refractive indices n_{inc} and n_{tr}. Diffraction orders will appear first and will be more numerous in media with higher refractive indices. These quantities are related together through the grating equation:

$$n_{tr}\sin[\theta(m)] = n_{inc}\sin\theta_{inc} - m\frac{\lambda_0}{p} \tag{2.19}$$

Adopting the free space as incident medium (n_{inc} = 1), we can calculate the total number of possible diffracted modes M as

$$M = \frac{2p}{\lambda}(\sin\theta_{inc} + n_{tr}) + 1 \tag{2.20}$$

Figure 2.3a depicts the maximum possible number of diffraction orders with respect to the coefficient p/λ for different values of refractive index n. As it was expected from the formula, the number of diffracted mode increases for higher values of n. Similarly, Figure 2.3b shows how wider incident angles lead to a larger number of diffracted modes.

(a) Normal incidence (θ_{inc} = 0°).

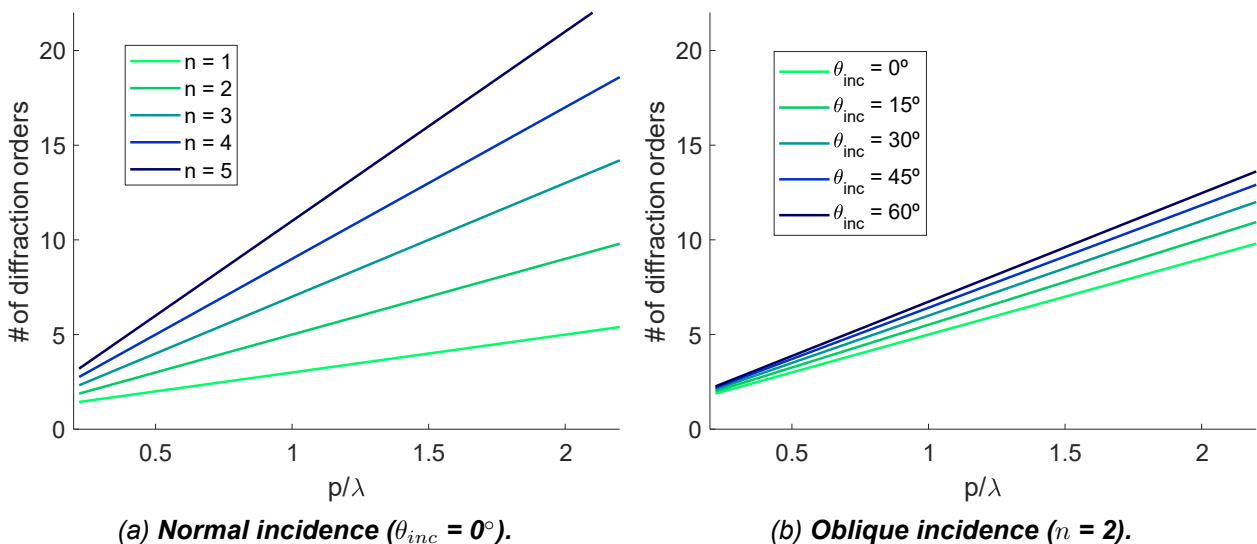*(b) Oblique incidence (n = 2).*

*Figure 2.3: **Diffraction orders for different refractive indices** n **and incidence angles** θ_{inc}.*

It is important to remark that the grating equation informs us about the number of possible diffracted modes, as well as their directions, for normal and oblique incidences, but it does not say anything about the amplitude and polarization of these modes. In order

to determine the diffraction efficiency and polarization of the diffraction orders, Maxwell's equations must be solved. Depending on the nature of the scatterers forming constituting the unit cell, specific analytical tools can be used to analyze the periodic structure. Throughout the following section, a focus will be made on structures formed by a periodic arrangement of resonators.

2.3 Periodic arrangement of dielectric resonators

2.3.1 Resonating principle

The notion of a resonator implies the existence of eigenmodes localized in space. In a closed resonator without dissipation, each mode is characterized by its resonant frequency (energy level) ω_{res} and spatial structure of the field $\chi(\mathbf{r})$. The eigenmode field Φ can be factorized as $\Phi(\mathbf{r}, t) = \Phi(t)\chi(\mathbf{r})$, where Φ is a solution of the harmonic-oscillator equation [5],

$$\frac{d^2\Phi}{dt^2} + w_{res}^2\Phi = 0 \tag{2.21}$$

Depending on whether the modes are localized in all spatial dimensions or not, the resulting spectrum can be either discrete or continuous. The resonator can be non-conservative due to internal dissipation of energy. Furthermore, the barriers can allow small energy leakage either from or to the cavity, e.g., due to "under-barrier" tunnelling via evanescent waves. In such cases, one has to consider the resonator as an open system with quasi-modes characterized by fuzzy energy levels of a finite width. The time dependence of the fields is not purely harmonic anymore and can be described as an oscillator with damping,

$$\frac{d^2\Phi}{dt^2} + w_{res}Q^{-1}\frac{d\Phi}{dt} + w_{res}^2\Phi = 0 \tag{2.22}$$

Here, the quality factor Q characterizes the total losses in the resonator, and it can be decomposed as follows:

$$Q^{-1} = Q_{diss}^{-1} + Q_{leak}^{-1} \tag{2.23}$$

where Q_{diss} and Q_{leak} are the quality factors responsible for the dissipation and leakage, respectively.

The type of structures we deal with in this work consist on a periodic arrangement of strongly coupled resonators made of a lossy material, as shown in Figure 2.4. Thus, the dissipation of energy (Q_{diss}) will be effectuated by means of material losses, represented by the material quality factor Q_d. If the resonator is made of a single material with permittivity ε_r and permeability μ_r, then the energy dissipation by material losses is given by the
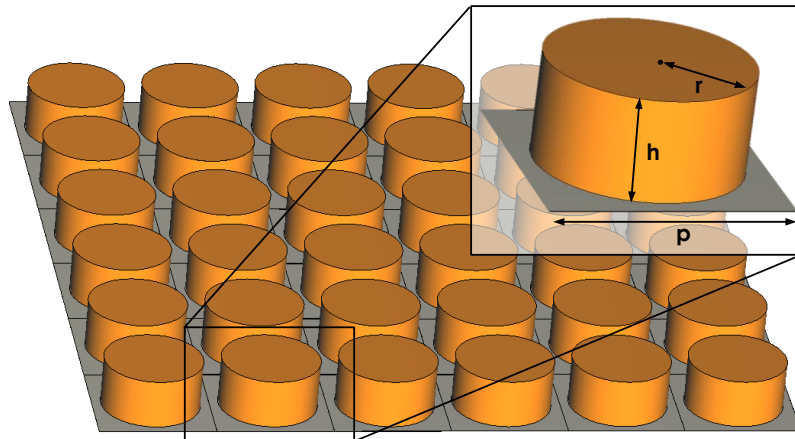
Figure 2.4: **Periodic structure made of cylindrical resonators. Geometrical parameters.**

material quality factor as

$$Q_{diss} = Q_d = \frac{1}{\tan\delta} = \frac{1}{\tan\delta_\varepsilon} + \frac{1}{\tan\delta_\mu} = \frac{\varepsilon'}{\varepsilon''} + \frac{\mu'}{\mu''} \tag{2.24}$$

where $\tan\delta_\varepsilon$ and $\tan\delta_\mu$ state for the dielectric and magnetic loss tangents, as defined in Section 2.2.1. On the other hand, the energy leakage from the resonator cavities is represented by the radiative quality factor $Q_{leak} = Q_{rad}$, that describes the coupling of resonators with free space. The total resultant quality factor Q_{tot} of the resonator model is given by

$$Q_{tot} = (Q_d^{-1} + Q_{rad}^{-1})^{-1} \tag{2.25}$$

The introduction of Q_{rad} and Q_d allows to reformulate the definition of reflection coefficient previously given in Equation 2.3 as

$$\Gamma = \frac{Q_d^{-1} - Q_{rad}^{-1}}{Q_d^{-1} + Q_{rad}^{-1}} \tag{2.26}$$

using the definition of resonant reflection coefficient given in [6]. This provides a useful way of calculating Γ at the resonant frequency of resonating structures.

Since the resonators will be arranged in a periodic manner, it is interesting to analyze the impact of the proximity of resonators on the coupling between them, that will determine the value of the radiative quality factor Q_{rad} at the resonance. In order to study the dependency of period variations on the radiative quality factor of a resonating mode of a cylindrical resonator, the same resonator geometry ($l = h = 10$ mm) is preserved and the period of the unit cell is varied.

The obtained distribution of Q_{rad} is showed in Figure 2.5. For $p > 30$ mm, a quadratic dependence of Q_{rad} on the period is observed. In this way, the radiative quality factor
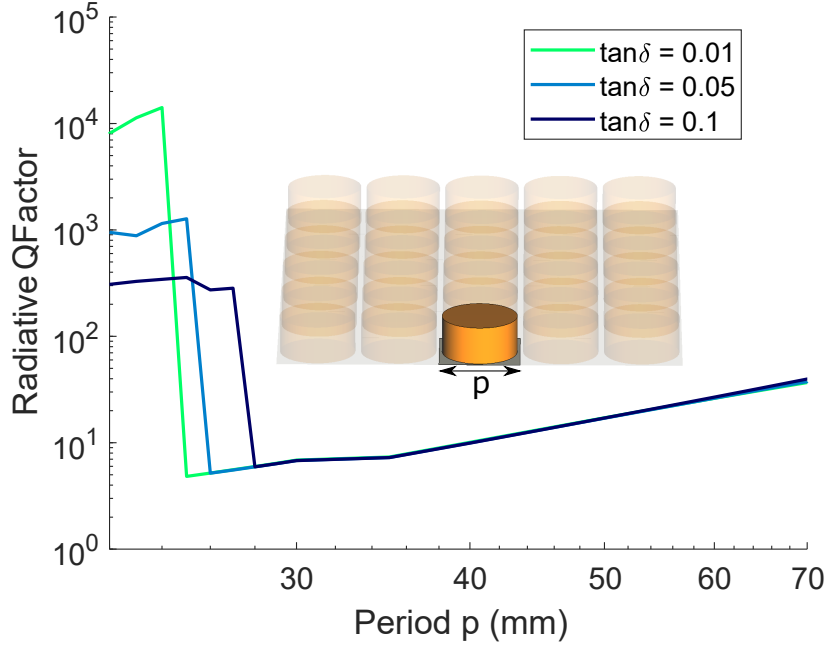
Figure 2.5: **Dependency of period variations on radiative quality factor** Q_{rad}**.**

tends to infinity when the resonators are very distant from each other. This is logical, given that when the period is much larger than the length of the resonators, they are almost not coupled. On the other hand, when $p < 30$ mm, the coupling between resonators strongly increases and it modifies the total quality factor Q_{tot}. The same analysis is performed for three different levels of loss tangents: 0.01, 0.05, 0.1. One can clearly observe that Q_{rad} is very similar for all levels of losses, which will allow us in the future to assume Q_{rad} to be independent of material losses.

2.3.2 Resonator geometry

The resonant frequency depends on the resonator size and geometry, as well as on its material properties. This information is contained for a specific field distribution in the characteristic equation of the resonating mode, that is obtained after solving Maxwell's equations applying boundary conditions at the interface of the resonator cavity. On the following, we consider a cylindrical resonator shape, and the HEM_{11} as the excited mode. Here, the nomenclature proposed by Kajfez [7] is adopted, using cylindrical coordinates (ρ, θ, ϕ), where the HEM_{11} mode presents an hybrid nature with respect to the axis of rotation. The expression of the resonant frequency of the HEM_{11} mode in the cylinder is given by [8]

$$k_0 r = \frac{6.324}{\sqrt{\varepsilon_r + 2}} \left[0.27 + 0.36 \left(\frac{r}{2h} \right) + 0.02 \left(\frac{r}{2h} \right)^2 \right] \qquad (2.27)$$

where r and h state for the radius and height of the cylinder, respectively, as indicated in

Figure 2.4. The the **E** and **H** field distributions of the HEM_{11} mode are shown in Figure 2.6. One can observe how the far field radiation of such a mode is equivalent to the one of a magnetic dipole orientated in the radial direction.
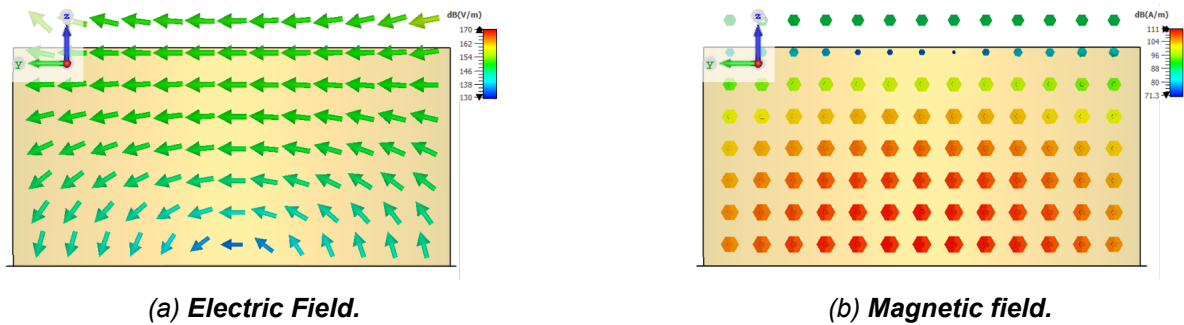

(a) Electric Field.

(b) Magnetic field.

*Figure 2.6: **Field distribution of HEM_{11} mode excited in a cylindrical resonator.***

Figure 2.7a illustrates the dependence between the HEM_{11} mode resonant frequency and the size and material properties of the resonator. The radius r and the permittivity ε_r (it should be noted that a purely dielectric material is adopted, hence $\mu_r = 1$) are varied, and the resonant frequency is calculated in simulation using the Eigenmode solver of CST. The period of the unit cell is set to be $p = 2r + 2$ mm, aiming to keep a similar coupling level for all simulated configurations. It can be observe that, for every value of r, the resonant frequency curve fits into a potential distribution of the type $y = kx^{exp}$, where $exp < 0$. Moreover, the curves are shifted towards lower frequencies as the radius of the cylinder increases. Such an analysis can result to be very useful when choosing the adequate resonator geometry given the desired frequency band of operation and material properties.
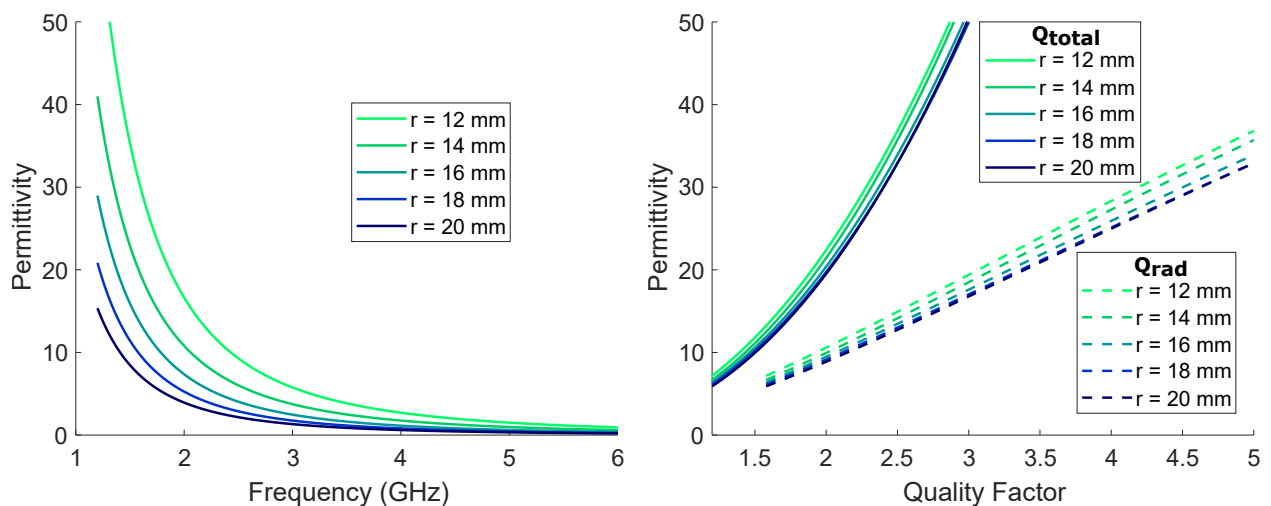
(a) Mode HEM_{11} resonant frequency vs permittivity for different cylinder radii.

(b) Mode HEM_{11} total and radiative quality factors vs permittivity for different cylinder radii.

*Figure 2.7: **Field distribution of HEM_{11} mode excited in a cylindrical resonator.***

Pablo H. Zapata Cano

Similarly, the quality factor at the resonance is extracted from simulation for the same permittivity and radius values in Figure 2.7b. Since the material losses remain the same for all curves ($\tan\delta = 0.2$, which gives a fixed material quality factor Q_d of 5), Q_{rad} can be derived from the total quality factor (dashed lines on the Figure) using Equation 2.25. It is observed how Q_{rad} linearly augments with permittivity, which means that resonators are less coupled when permittivity increases.

The same analysis can be carried on for hemispherical resonators. In this case, the excited mode is named as TE_{111} (equivalent to the HEM_{11} mode for cylindrical coordinates), in which the electrical field is transverse to the normal vector of the surface of the hemisphere. The resonant frequency f_{res} of such a mode is obtained from the following characteristic equation [9]:

$$\frac{k_0 r \sqrt{\varepsilon_r}\,\mathcal{J}_1(k_0 r \sqrt{\varepsilon_r})}{\left[k_0 r \sqrt{\varepsilon_r}\,\mathcal{J}_1(k_0 r \sqrt{\varepsilon_r})\right]'} = \sqrt{\varepsilon_r}\,\frac{k_0 r \mathcal{H}_1^{(2)}(k_0 r)}{\left[k_0 r \mathcal{H}_1^{(2)}(k_0 r)\right]'} \tag{2.28}$$

as

$$f_{res}(GHz) = \frac{4.7713 Re(k_0 r)}{r(cm)} \tag{2.29}$$

where $\mathcal{J}_1$ and $\mathcal{H}_1^{(2)}$ refer to first-type spherical Bessel functions and spherical Hankel function of the second kind, respectively, and r corresponds to the radius of the hemisphere. The electric and magnetic field distributions inside the resonator when the TE_{111} mode excited are illustrated in Figure 2.8
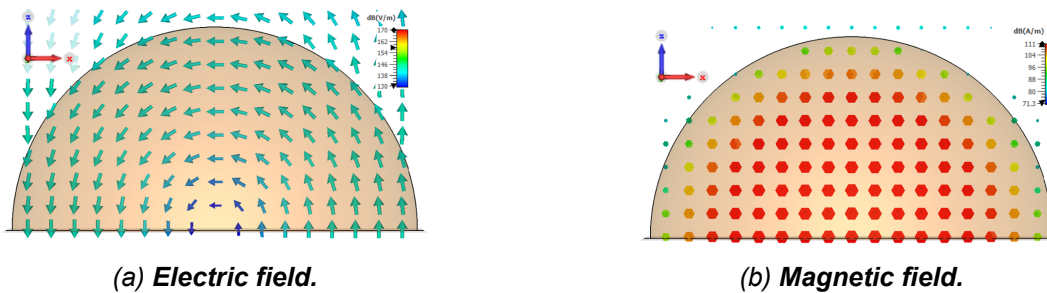

(a) *Electric field.*   (b) *Magnetic field.*

Figure 2.8: **Field distribution of** TE_{111} **mode excited in a hemispherical resonator.**

Figure 2.9 shows a comparison of the mode resonant frequency for both the cylindrical and hemispherical resonators. The parameter r on the figure states for both the radius of the hemisphere and the radius of the cylinder. Moreover, the height of the cylinder has also been set to be equal to its radius (i.e. $h = r$).

One can observe how the distributions are very similar, being the one of the cylinder slightly shifted towards lower frequencies. This can be explained by the fact that the volume of the hemisphere is lower than the one of the cylinder. In fact, if the same analysis is conducted
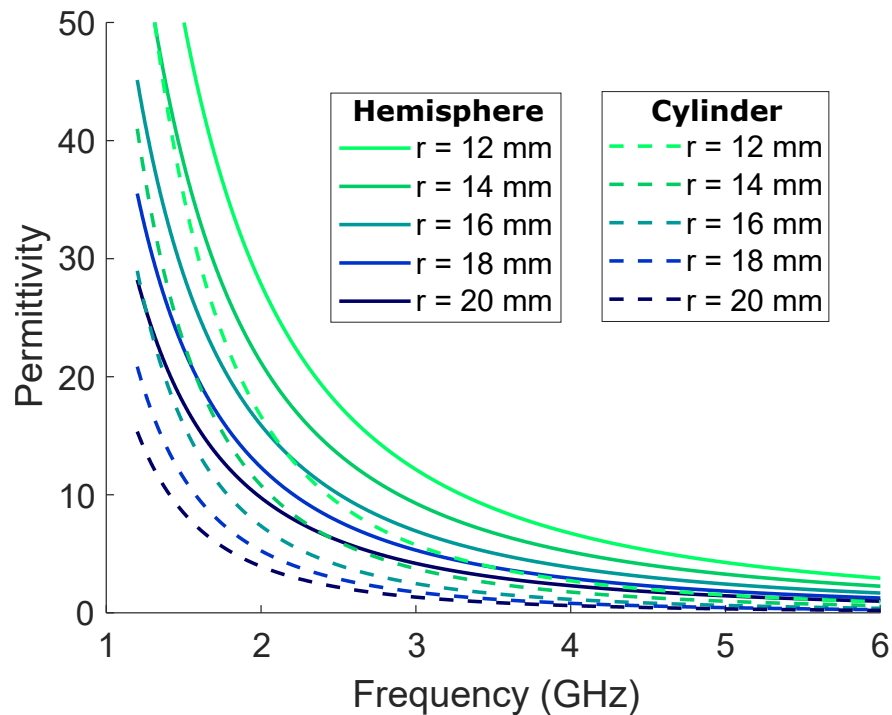
Figure 2.9: **Resonant frequency vs permittivity for cylindrical and hemispherical resonators.**

for resonators of equivalent volumes, the resonant frequencies of the cylinder and the sphere would be identical.

2.3.3 Functionalities of periodic structures made of dielectric resonators

Periodic structures composed by the arrangement of dielectric resonators result to be of great interest for practical applications that imply wave manipulation and/or filtering or absorption. Moreover, they present large design flexibility and reduced space.

Among the possible functionalities of this kind of structures, Frequency Selective Surfaces (FSS) can be used as spatial filters to transmit or reflect electromagnetic (EM) waves with different operating frequencies, polarizations and incident angles [10]. By using dielectric resonators to build FSS, the physical properties of such materials (relative permittivity, loss level...) can be used to modulate the EM transmission performance in an artificial route. Furthermore, all-dielectric materials result to be very suitable for high-power and high-temperature applications [11]. With the aim of meeting design demands, multiple materials and shapes can be explored [12], being possible to achieve artificial effective material properties, such us a negative permittivity and/or permeability.

In [13], a high-permittivity ($\varepsilon_r > 100$) ceramic material is used together with a flexible spatial arrangement to design an easily reconfigurable FSS in the X and Ku bands. As it is depicted in the Figure 2.10, four cubes made of a dielectric material are strategically arranged in space to modulate the resonance and thus achieve reconfigurable pass/stop
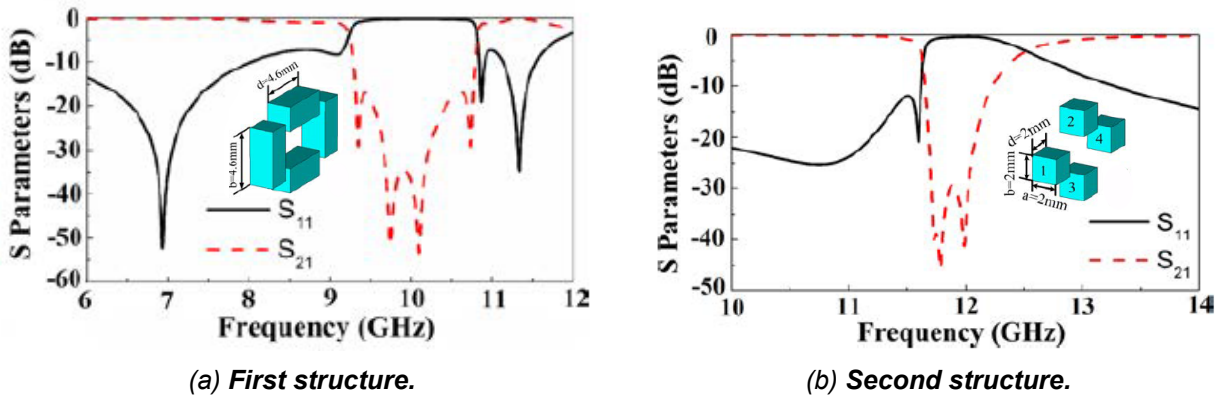
(a) **First structure.**

(b) **Second structure.**

Figure 2.10: **Design reconfigurability of the 3-D printed FSS proposed in [13].**

band effects by tuning the material permittivity and/or the parameters a, b or d. Then, a support is fabricated using 3-D printing to provide the structure with mechanical consistency. In fact, 3-D printing supports cost efficient design, precise modelling and easy non-planar manufacturing, plus an additional degree of freedom when it comes to structural design. This can also be exploited to explore multiple resonator shapes [14] or geometrically complex and non-intuitive designs of FSS. The later strategy is adopted in [15] to design a large bandwidth and field of view FSS by means of a genetic algorithm, utilizing all of the geometric freedom 3-D printing offers.

Microwave absorbers constitute another attractive application of such structures. In a similar way to FSS, the disposition, shape and material characteristics of the resonators are manipulated to meet design requirements, that can include broadband absorption, reduced thickness, and wide-angle or polarization robustness, among others. In fact, the main focus of this work relies on the realization of 3-D printed absorbers made of dielectric resonators. Thus, the next section of the manuscript is devoted to introduce the principle of absorption and present a deeper insight of the state of the art in this field.

3. ABSORBERS

This chapter contains the principles from which the absorptive capacities of the structures presented in this work are deduced. The adopted design strategy consists of using a periodic arrangement of scatterers with a determined geometry to artificially control the surface impedance, which subsequently means controlling the amount of energy that can be dissipated within the resonators, and hence the absorption level. This problem can be reformulated in several ways, with the aim of identifying and isolating the parameters playing a crucial role on the modification of the impedance. On top of that, the freedom given by the utilization of 3-D-printing techniques is exploited to tune the material properties of the resonators, as well as the coupling between them, accordingly to control the absorption level.

3.1 Absorption principle

Electromagnetic waves incident on a medium can either be reflected, transmitted or absorbed by the medium. Figure 3.1 depicts a basic schema of a structure composed by a single material (with electromagnetic properties ε_r and μ_r) on top of a PEC (Perfect Electric Conductor) plate. The presence of the metallic plate allows us to neglect transmission, being able to define the power absorption coefficient A as

$$A = 1 - \sum_{m=1}^{M} |\Gamma_m|^2 \tag{3.1}$$

where Γ_m stands for the reflection coefficient of the m diffracted order. The total number of modes M is given by the grating equation (Equation 2.20). Considering the definition of the reflection coefficient, provided in Equation 2.2, it is straightforward to state that the impedance matching between the two interfaces is crucial to achieve full absorption.

A perfect absorber is defined as the one that does not reflects any of the incident wave energy into its origin medium, i.e. all energy is dissipated in the absorbing medium. If the origin medium is the air (with an impedance $\eta_0 \sim 377\Omega$), the perfect absorption condition is fulfilled if $\eta = \eta_0$, being η the impedance of the absorbing medium. This, attending to the definition of characteristic impedance given in Equation 2.10, implies $\varepsilon_r = \mu_r$.

3.2 Derivation of the absorption level

As it was developed in Section 2.1, the calculation of the characteristic impedance η of the absorbing medium (and hence the derivation of an expression for the absorption level) is often not that intuitive, and depend on many factors such as the frequency of operation, the geometry of the structure or the angle of incidence of the wave. For example, if we
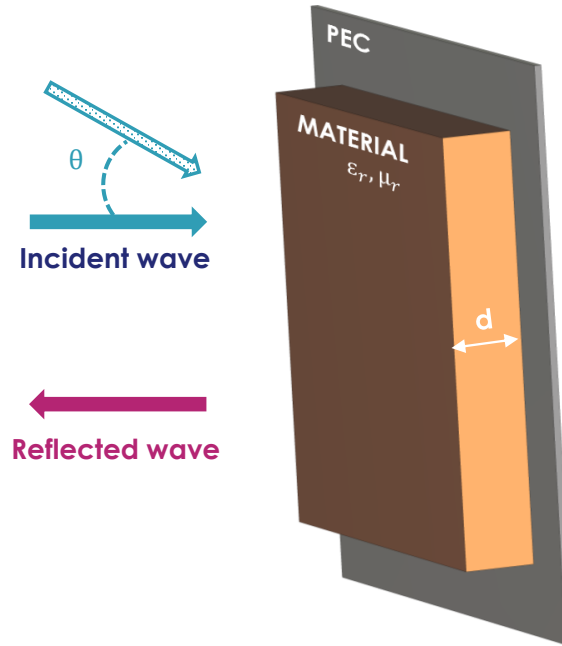
Pablo H. Zapata Cano

Figure 3.1: **Incident and reflected waves on a material on top of a PEC plate.**

consider a resonator with a geometry like the one depicted in Figure 3.1, transmission line theory can be applied to calculate the impedance of the structure. The general expression of Equation 2.4 becomes the one of a short-circuited line [16], in which the load impedance is 0 and the characteristic impedance of the medium is η. Then, Equation 2.3 gives us the correspondent reflection coefficient, that results into the following expression for the absorption level using Equation 3.1 (normal incidence of waves at the interface is considered):

$$A = 1 - \left| \frac{\sqrt{\frac{\mu_r}{\varepsilon_r}} \tanh \left(j \frac{2\pi f d}{c} \sqrt{\varepsilon_r \mu_r} \right) - 1}{\sqrt{\frac{\mu_r}{\varepsilon_r}} \tanh \left(j \frac{2\pi f d}{c} \sqrt{\varepsilon_r \mu_r} \right) + 1} \right|^2 \tag{3.2}$$

However, obtaining an analytical expression for the characteristic impedance can result to be really challenging for more complex (layered, multimaterial) structures and oblique incidence angles. In those cases, other approaches like the derivation of material properties using effective medium theory (when applicable, see Section 2.2.2) can be of great interest.

An equivalent analysis, considering the resonant behavior of the structure, can result to be very convenient in some cases when the periodic structure is formed by an arrangement of resonators. Adopting the material and radiative quality factors previously introduced in 2.3.1, and using the expression of the reflection coefficient of Equation 2.26, the absorption

level can be expressed as [17]

$$A = 1 - \frac{\left[Q_d^{-1} - Q_{rad}^{-1}\right]^2}{\left[Q_d^{-1} + Q_{rad}^{-1}\right]^2} \tag{3.3}$$

If we define the coefficient α as the ratio of both radiative and material quality factors ($\alpha = Q_{rad}/Q_d$), it is straightforward to state that the absorption will be maximum (unitary absorption coefficient) when α = 1 (i.e. $Q_{rad} = Q_d$). This formulation also allows us to express the absorption in terms of α for any target absorption level A_{target}:

$$A_{target} = 1 - \left(\frac{\alpha - 1}{\alpha + 1}\right)^2 \tag{3.4}$$

Using this expression, α can be deduced for any target absorption level as

$$\frac{\alpha - 1}{\alpha + 1} = \pm\sqrt{1 - A_{target}}, \quad \alpha = \begin{cases} \alpha_+ = \frac{1+\sqrt{1-A_{target}}}{1-\sqrt{1-A_{target}}} & \Rightarrow Q_{rad} \geq Q_d \\ \alpha_- = \frac{1-\sqrt{1-A_{target}}}{1+\sqrt{1-A_{target}}} & \Rightarrow Q_{rad} \leq Q_d \end{cases} \tag{3.5}$$

When the absorption coefficient is not unitary, i.e. $Q_{rad} \neq Q_d$, we distinguish two possible scenarios: domination of material losses (material quality factor lower than radiative quality factor) or domination of coupling losses (coupling quality factor lower than material quality factor). Given the type of structures we deal with in this work, in which the resonators are strongly coupled, coupling losses will dominate, and hence $\alpha = \alpha_-$. In that case, and assuming that coupling (Q_{rad}) is independent of variation of material losses (Q_d), an equivalent $Q_{d_{target}}$ for a given target absorption level A_{target} can be obtained from

$$Q_{d_{target}} = \frac{Q_{rad}}{\alpha}, \quad where \quad \alpha = \alpha_- = \frac{1 + \sqrt{1 - A_{target}}}{1 - \sqrt{1 - A_{target}}} \tag{3.6}$$

This will allow us to control the absorption level for a fixed resonator structure, just by changing the losses of the material from which the resonators are made.

3.3   State of the art. Microwave absorbers

In this work, periodic arrays made of lossy resonators are used for the conception of structures capable of controlling the absorption level of energy over a broad frequency band. However, other techniques have been used in the literature for the design of microwave absorbers. Among them, Salisbury [18] and Jauman [19] screens utilize resistive losses for energy dissipation, while the Dallenbach screen [20] follows a similar principle exploiting dielectric losses. Several materials with different chemical properties are employed with the aim of adequately tuning the imaginary portions of the electric permittivity and the magnetic permeability to achieve the desired absorption level. However, these solutions suffer from a narrow bandwidth and poor mechanical robustness. In order to tackle that, periodic structures are largely employed in the literature. Compared to a resistive sheet, the added value of periodic surfaces is that their impedance is not purely real but complex, which can be exploited to generate additional resonant behaviours [21].

Periodic structures consisting on the arrangement of resonators allow to achieve absorption by means of energy dissipation inside the resonating structures and the coupling between them. In this line, multiple solutions have been explored in terms of resonator shapes and materials. Dielectric [22] and magnetic [23] resonators, often configured on a layered topology, have been used to achieve broad band absorption. Moreover, dispersive material properties can be exploited to broaden the frequency bandwidth. Following this principle, a >90% absorption over the 4-40 GHz band is achieved in [24]. Furthermore, the concatenation of multiple mode resonances can also contribute to achieve a broadband behaviour. This principle has been exploited in [25], achieving a reflectivity of less than -20 dB in the X-band.

Recent advances of nanomaterial engineering [26] has contributed to the exploration of new materials, that can also be used for microwave absorption applications [27]. For example, flexible graphene composites are used in [28], reaching more than 97% absorption over a 62.73 GHz bandwidth. Furthermore, 3-D printing [29] provides low-cost and monolithic manufacturing process as well as other interesting design characteristics such as mechanical strength, modularity and conformability [30]. In addition, the combination of additive manufacturing with the synthesis of new materials through the utilization of loaded composites and polymers [31] provides many degrees of freedom for the design in terms of material properties and geometry. This has been exploited to build stacked structures [32], in which multiple materials are combined [33]. Wide-angle- and polarization-robustness is still a challenge for microwave absorbers operating over a large bandwidth. In order to tackle this, some of the techniques introduced above have been put together in the design of metamaterial absorbers [34] [35]. However, they are still very narrowband.

In Table 3.1, three microwave absorbers from representative works in the literature are compared. In order to do so, three performance indicators are defined, aiming for a wideband, thin and wide-angle robust absorber. These are:

- Bandwidth of operation $f_{min} - f_{max}$, complemented by the fractional bandwidth $FBW = 2(f_{max} - f_{min})/(f_{max} + f_{min})$, for an absorption level above 0.9 (90%).

- Thickness of the structure with respect to wavelength at lowest frequency f_{min}

- Performance at oblique incidence: Maximum angle for which an absorption level of 0.8 (80%) is reached over the operation band. Correspondence between TM and TE polarizations.
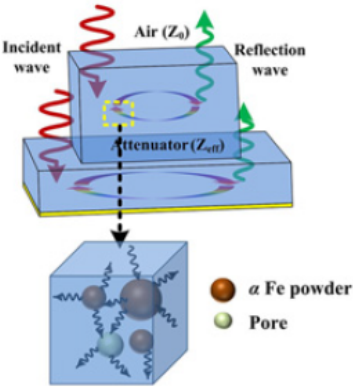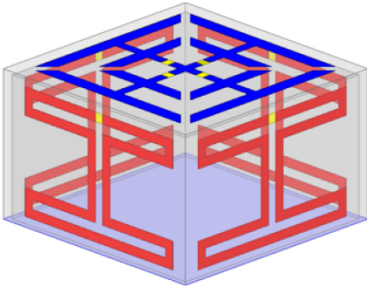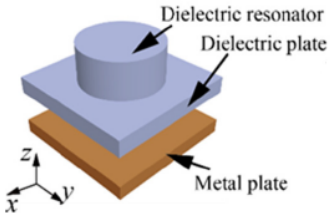
Work	Specifications	Details	3-D
Zhou, Yin et. al. [23]	→ FBW = 175% (from 2.64 to 40 GHz) → Above 80% absorption reached for all angles until 45° → Thickness of 0.048λ at lowest frequency	✓ Ultra-broadband absorption ✓ Thin thickness ✗ Hard to control absorption level	✗
Shi, Han et. al. [34]	→ FBW = 61% (from 2.07 to 3.89 GHz) → Above 80% absorption reached for all angles until 60° → Thickness of 0.09λ at lowest frequency	✓ Dispersion and dissipation analysis ✓ Polarization-Independent ✗ Very narrowband (1.78 GHz bandwidth)	✗
Ren, Yuan et. al. [31]	→ FBW = 102% (from 3.9 to 12 GHz) → Above 83% absorption reached for all angles → Thickness of 0.12λ at lowest frequency	✓ Cheap and easy manufacturing ✓ Resonance modelling by dielectric resonator ✗ Only unitary absorption level	✓

Table 3.1: Comparison of selected microwave absorbers in the literature.

Pablo H. Zapata Cano

As it can be deduced from the table, these three designs present promising solutions that achieve very good performances in terms of operating bandwidth, structure thickness or wide-angle robustness, depending on the case. Nevertheless, it is still challenging to accomplish good levels for all performance indicators at the same time. For example, absorber presented in [34], despite of showing very competitive figures of merit regarding polarization invariance and wide-angle robustness, exhibits a bandwidth of 1.79 GHz, which is still very far from the one targeted by the structures developed in this work. Also, the arduous and costly manufacturing of some of the presented absorbers is sometimes a constraint to consider for some specific applications. To this regard, 3-D-printed-absorbers state as a rising alternative which provides design flexibility and a simple and cheap manufacturing. Finally, it should be remarked that all these devices are conceived with the aim of reaching a unitary absorption level. However, sometimes the goal is to control the amount of energy that is absorbed. This implies a deep understanding of the absorption mechanism of the device, as well as of the physical phenomena causing the energy dissipation. With respect to that, structures formed by the concatenation of resonators (scatterers) give the degrees freedom needed to perform this control, achieved through geometric variations of the structure or profiting from the wide range of available materials accessible by 3-D-printing.

4. SIMULATION AND MEASUREMENT SETUPS

In this chapter, the software and hardware tools, as well as some procedures adopted for the development of the solutions proposed on this work, are listed and presented.

4.1 Full wave simulation of periodic structures

For the simulation of the structures studied in this work, the commercial software CST Microwave Studio Suite is used. The configuration of boundaries chosen to simulate periodic structures with resonators is depicted in Figure 4.1.
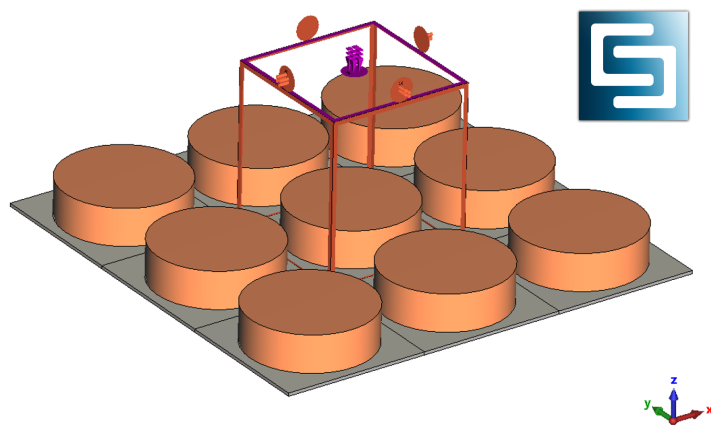

Figure 4.1: **Simulation configuration of a periodic structure composed of cylindrical resonators in CST Studio Suite.**

Unit cell boundaries are chosen to emulate an infinite array of resonators along the x and y directions. For the z axis, open cell boundaries are chosen on the side of the resonators, whereas a PEC plate together with electric boundary conditions avoid any transmission on the other side. With this configuration, Floquet ports are considered, each of which corresponds to a direction of propagation of a plane wave incident to the structure. The number of Floquet modes to contemplate must be set to the simulator, and it is determined through a convergence test, keeping in mind the considerations made in Section 2.2.3. In this way, a number of modes large enough to include all diffracted energy in the calculation of the absorption is found, trying to reduce the simulation time as much as possible.

Sometimes, when studying the resonant behaviour of a structure, the Eigenmode solver of CST is used instead of the frequency solver, which permits to calculate the frequency and quality factors of the excited mode, and study the nature of the electromagnetic fields in the cavity by observing the field distribution. In order to do that while considering a periodic structure, periodic boundary conditions are set along the x and y axis, and the "Eigenmode Lossy" option of the solver is selected.

         Pablo H. Zapata Cano

4.2   Bistatic characterization at normal and oblique incidence

The characterization of the fabricated absorbers is done in a semi-anechoic environment. As shown in Figure 4.2, bistatic measurements are performed to measure the reflection of the structure at normal and oblique angles of incidence. Two wide band horn antennas (Satimo QR2000) operating in the 2-18 GHz frequency are installed at the extremes of two articulated arms. As showed in the picture, the position of the antennas is symmetrically varied at the same time that the sample is rotating, which allows to conduct measurements for incident θ_i angles ranging from 0 to 70 °.
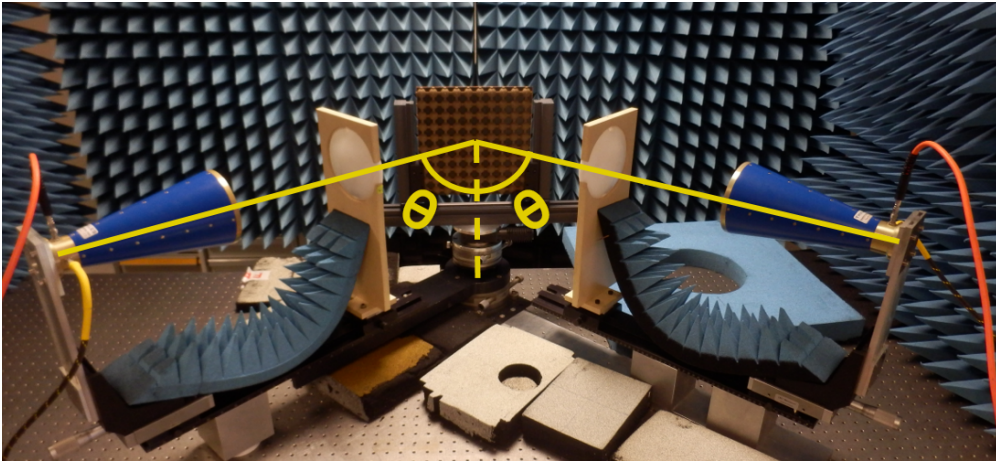

*Figure 4.2: **Characterization set up (for $\theta_i = 45°$ and an absorber used as a sample).***

Although classical pyramidal absorbers are placed around the equipment to mitigate any interference, a calibration operation is performed in order to eliminate the effect of the environment on the measurement [36]. Thus, the reflection coefficient is deduced as follows:

$$RL_{dB} = 20 \log_{10} \left(\frac{RL^{absorber} - RL^{freespace}}{RL^{freespace} - RL^{metal}} \right) \tag{4.1}$$

where $RL^{absorber}$, RL^{metal}, $RL^{freespace}$ correspond to the transmission coefficients from one antenna to the other when the absorber, a metallic plate and the air is used as the sample, respectively. Moreover, two lens are incorporated between the antennas and the structure in order to focalise the radiated fields towards the sample, augmenting the directivity of the antenna.

Figure 4.3 illustrates the influence of the distance between each lens and its respective antenna on the transmission. It shows the transmission coefficient between the two aligned antennas that are symmetrically positioned with respect to the central point (where the sample will be positioned afterwards). It can be clearly appreciated that almost 20 dB is gained when the lens is separated more than 7 cm from the antenna. This is especially relevant at high frequencies of operation.

Also, it is worth mentioning that a time domain post-processing is sometimes applied to

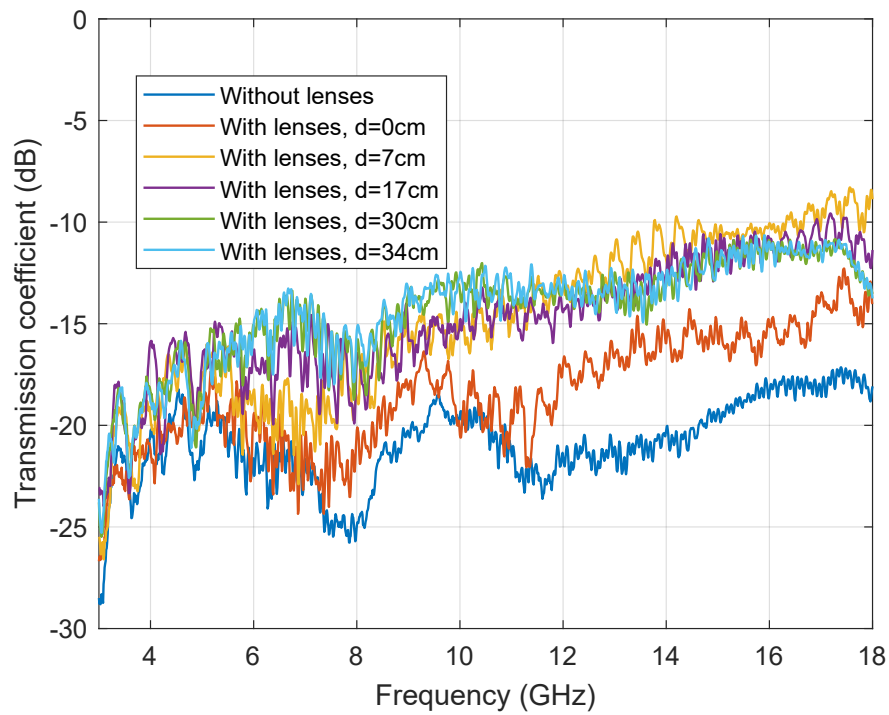*Figure 4.3:* **Impact of the positioning of the lenses.** d **corresponds to the distance between the lenses and the antennas.**

the characterization results. It consist on a temporal Hamming-window-shaped filter that is applied to the measured signal, with the objective of isolating only the useful signal and eliminate any other reflection/multipath replica of the transmitted signal.

4.3   Material characterization

Through the material characterization process, the electromagnetic properties of a material are determined. In the microwave range, several methods based on reflection, transmission or transmission/reflection are used. All these methods work in free space, coaxial line, waveguide, or resonant cavity. The choice of the technique of measurement and the retrieving methods depend on the sample to characterize. The material characterizations presented in this work are conducted using a coaxial line cell equipped with a containment area. Then, the material relative permittivity $\varepsilon_r = \varepsilon' - j\varepsilon''$ and permeability $\mu_r = \mu' - j\mu''$ are extracted from the scattering parameters of a sample via the Nicolson-Ross method as described in [37].
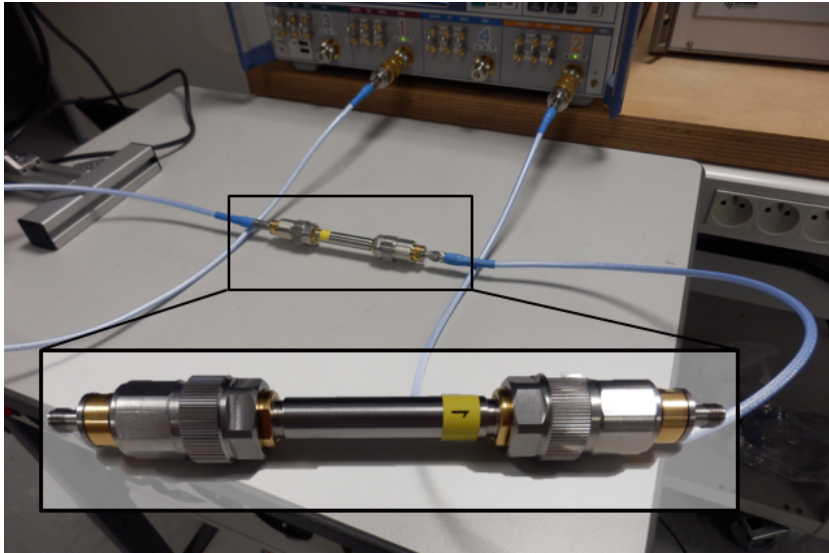

Figure 4.4: ***Set-up for material characterization.***

Figure 4.4 shows the material characterization set-up. The sample to characterize is inserted inside on the cavity of the EpsiMu tool-kit. This makes a sort of coaxial line configuration, the ends of which are connected to two different ports of a Network Vector Analyser (VNA), used to extract the S-parameters that will be processed.

5. BROADBAND ABSORPTION CONTROL

Understanding the physical phenomena that produce absorption is an essential step for the development of design and analysis procedures of structures with absorbing capabilities. Through this chapter, some of the theoretical basis previously introduced in Section 3.1 are applied to build a design procedure that allows for the control of the absorption level over a large range of frequencies. Two main approaches are adopted: On the one hand, artificially generated materials with particular dispersion behaviours are used in Section 5.1. Following this principle, broadband absorption is achieved through the prolongation of the excited mode in the resonator cavity. On the other hand, Section 5.2 presents a method in which optimization is used as a design engine to combine multiple materials in a stacked geometry, always with the same goal of controlling absorption.

5.1 Extended mode excitation through material dispersion

In this section, a periodic structure formed by the concatenation of hemispherical resonators is adopted. The combination of this geometry with 3-D-printing manufacturing provides a number of degrees of freedom that make it possible to develop a design method in which both the dissipation of energy in the resonators and the coupling between them are tuned to regulate the absorption level. In this work, this is done by the design of a single material with special dispersive properties, that is integrated into an hemispherical resonator design.

The result is a periodic architecture in which absorption is controlled by changing the properties of the material used for manufacturing. This benefits of both the geometrical and electromagnetic (material properties) degrees of freedom provided by 3-D printing additive manufacturing.

5.2 Multi-material absorber design via optimization

In this section, an optimization-based strategy is presented for the design of wideband absorbers through the combination of multiple materials on a stacked structure.

Since the early 90s [38], optimization techniques have been applied to the design of absorbing structures. Among them, genetic algorithms [39] and other advance metaheuristics are widely used to address problems like improving the absorption capability at normal and/or oblique incidence or reducing the thickness of the structure. These objectives are often jointly formulated [40] in a single function, which allows to avoid the long and resource-consuming multi-objective approaches.

Optimization is also widely applied together with full-wave simulators, resulting very useful for the final stage of the design, in which multiple parameters are tuned to find an optimal

solution. Nevertheless, this can be extremely time-consuming when the number of iterations is high, specially for broadband applications, where many frequency points need to be evaluated. In order to tackle that, analytical or numerical methods are a powerful tool that allows to reduce drastically the overall simulation time. Among them, the Fourier Modal Method (FMM) [41, 42] constitutes a rigorous solution providing competitive computational cost to simulate the interaction of electromagnetic waves with periodic interfaces. In [43], the FMM is used for modeling pyramidal absorbers.

On the following, the FMM is used to model periodic structures made of stacked layers, whose optimal geometry and material properties are determined through optimization. Thus, a stacked geometry containing by five squared layers with decreasing size from the base to the top is adopted, constituting a pyramidal shape. Each of the five layers is made of a different dielectric material. The principle behind this arrangement is to exploit the multilayer geometry to create multiple resonances, with the aim of concatenating them to achieve broadband absorption. In order to do so, the physical dimensions and material properties of each layer are tuned to reach a certain absorption level over the whole frequency band. In this way, absorption is controlled over a large band of frequencies, and the simulation time is drastically reduced thanks to the utilization of the FMM, if we compare it with the one provided by full wave simulators.

6. FABRICATED 3-D-PRINTED BROADBAND ABSORBER

This chapter is devoted to the design, fabrication and characterization details of a demonstrator consisting of a microwave absorber made of commercial materials. Hanoi-Tower-shaped resonators, fabricated using additive manufacturing with a 3-D-printable dielectric, are deposited on a magnetic elastomeric material to form the final structure. Exploiting the resonating modes in the hemispherical cavities, broadband absorption is achieved. The magnetic base helps in absorbing oblique incidence angles, especially for the TM polarization, and benefits from high magnetic losses to improve the impedance matching.

The results obtained in this chapter are synthesized on a scientific paper that is submitted to the 16th European Conference on Antennas and Propagation (EuCAP), that will be held in 2022 in Madrid (Spain).

7. CONCLUSIONS AND FUTURE WORK

This section summarizes the main results of this work, and provides some insights for possible future lines that might be exploited on the future.

Some of the most remarkable achievements of this Master Thesis includes:

- Two different approaches to design absorbers with a controllable absorption level using periodic structures have been proposed, based on the study of state-of-the art existing solution and theoretical analysis of this kind of structures.

- Absorption control over a large bandwidth is achieved with periodic structures made of dielectric resonators with dispersive properties. However, the performance of the design for wide oblique angles of incidence can still be improved

- Absorption control over a large bandwidth is achieved with periodic structures using a multilayer architecture. The design is obtained via optimization, using the FMM as an alternative to full wave simulators to reduce the evaluation time.

- A prototype has been designed, manufactured and characterized. It consists on a microwave absorber in which commercial materials are combined, profiting from the degrees of freedom given by 3-D printing.

Some of the possible future lines to explore are:

- Analytical and physical study of the coupling between resonators, and its dependence to the incidence angle and polarization state.

- Adaptation of the proposed method to magneto-dielectric materials (up until now, only dielectric losses and a permittivity dispersive profile was considered).

- Exploration of new optimization algorithms and/or specific operators to achieve better and/or less consuming optimization results.

- Conception and manufacturing of new prototypes in which new, more complex, synthesized materials are used instead of the commercial ones to enhance the performance of the proposed absorber.

REFERENCES

[1] S.J. Orfanidis. *Electromagnetic Waves and Antennas.* Rutgers University, New Brunswick, NJ, 2002.

[2] Chen, Grzegorczyk, Wu, Pacheco, and Kong. Robust method to retrieve the constitutive effective parameters of metamaterials. 70, Jul 2004.

[3] D. Schurig, J. J. Mock, and D. R. Smith. Electric-field-coupled resonators for negative permittivity metamaterials. *Applied Physics Letters*, 88(4):041109, 2006.

[4] J.B. Pendry, A.J. Holden, D.J. Robbins, and W.J. Stewart. Magnetism from conductors and enhanced nonlinear phenomena. *IEEE Transactions on Microwave Theory and Techniques*, 47(11):2075–2084, 1999.

[5] Konstantin Y. Bliokh, Yury P. Bliokh, Valentin Freilikher, Sergey Savel'ev, and Franco Nori. Colloquium: Unusual resonators: Plasmonics, metamaterials, and random media. *Rev. Mod. Phys.*, 80:1201–1213, Oct 2008.

[6] D. Bohm. *Quantum Theory*. Prentice-Hall, New York, 1951.

[7] D. Kajfez, A.W. Glisson, and J. James. Computed modal field distributions of isolated dielectric resonators. In *1984 IEEE MTT-S International Microwave Symposium Digest*, pages 193–195, 1984.

[8] R. Mongia and P. Bhartia. Dielectric resonator antennas—a review and general design relations for resonant frequency and bandwidth. *International Journal of Microwave and Millimeter-wave Computer-aided Engineering*, 4:230–247, 1994.

[9] A.A. Kishk, G. Zhou, and A.W. Glisson. Analysis of dielectric-resonator antennas with emphasis on hemispherical structures. *IEEE Antennas and Propagation Magazine*, 36(2):20–31, 1994.

[10] Ben A. Munk. *Frequency Selective Surfaces: Theory and Design*. John Wiley and Sons, New York, 2000.

[11] J. H. Barton, C. R. Garcia, E. A. Berry, R. G. May, D. T. Gray, and R. C. Rumpf. All-dielectric frequency selective surface for high power microwaves. *IEEE Transactions on Antennas and Propagation*, 62(7):3652–3656, 2014.

[12] Jun Wang, Shaobo Qu, Liyang Li, Jiafu Wang, Mingde Feng, Hua Ma, Hongliang Du, and Zhuo Xu. All-dielectric metamaterial frequency selective surface. *Journal of Advanced Dielectrics*, 07(05):1730002, 2017.

Pablo H. Zapata Cano

[13] Liyang Li, Jun Wang, Mingde Feng, Hua Ma, Jiafu Wang, Hongliang Du, and Shaobo Qu. All-dielectric metamaterial frequency selective surface based on spatial arrangement ceramic resonators. *Journal of Advanced Dielectrics*, 07(02):1750009, 2017.

[14] R. Adeline Mellita, S. S. Karthikeyan, and P. Damodharan. Additively manufactured conformal all-dielectric frequency selective surface. In *2020 50th European Microwave Conference (EuMC)*, pages 772–775, 2021.

[15] Jay H. Barton, Cesar R. Garcia, Eric A. Berry, Rodolfo Salas, and Raymond C. Rumpf. 3-d printed all-dielectric frequency selective surface with large bandwidth and field of view. *IEEE Transactions on Antennas and Propagation*, 63(3):1032–1039, 2015.

[16] J. Kong. *Electromagnetic Wave Theory*. EMW Publishing, Cambridge, Massachusetts, USA, 1986.

[17] Nicolas Fernez, Ludovic Burgnies, Jianping Hao, Colin Mismer, Guillaume Ducournau, Didier Lippens, and Éric Lheurette. Radiative quality factor in thin resonant metamaterial absorbers. *IEEE Transactions on Microwave Theory and Techniques*, 66(4):1764–1772, 2018.

[18] W.W. Salisbury. Absorbent body for electromagnetic waves, U.S. Patent 2 599 944, Jun. 1952.

[19] L.J. Du Toit. The design of jauman absorbers. *IEEE Antennas and Propagation Magazine*, 36(6):17–25, 1994.

[20] W. Dallenbach and W. Kleinsteuber. Reflection and absorption of decimeter-waves by plane dielectric layers. *Hochfreq. u Elektroak*, pages 152–156, 1938.

[21] Daniel Sjöberg. Analysis of wave propagation in stratified structures using circuit analogues, with application to electromagnetic absorbers. *European Journal of Physics*, 29(4):721–734, may 2008.

[22] Jianwen Xie, Sakib Quader, Fajun Xiao, Chong He, Xianling Liang, Junping Geng, Ronghong Jin, Weiren Zhu, and Ivan D. Rukhlenko. Truly all-dielectric ultrabroadband metamaterial absorber: Water-based and ground-free. *IEEE Antennas and Wireless Propagation Letters*, 18(3):536–540, 2019.

[23] Qian Zhou, Xiaowei Yin, Fang Ye, Xiaofei Liu, Laifei Cheng, and Litong Zhang. A novel two-layer periodic stepped structure for effective broadband radar electromagnetic absorption. *Materials and Design*, 123:46–53, 2017.

[24] Wei Li, Tianlong Wu, Wei Wang, Pengcheng Zhai, and Jianguo Guan. Broadband patterned magnetic microwave absorber. *Journal of Applied Physics*, 116:044110, 07 2014.

[25] Sofian Hamid and Dirk Heberling. Design of an x-band microwave magnetic absorber composed of multimode dielectric resonator array. In *2018 Asia-Pacific Microwave Conference (APMC)*, pages 684–686, 2018.

[26] Michael Green and Xiaobo Chen. Recent progress of nanomaterials for microwave absorption. *Journal of Materiomics*, 5(4):503–541, 2019.

[27] Yixing Huang, Wei-Li Song, Changxian Wang, Yuannan Xu, Weiyi Wei, Mingji Chen, Liqun Tang, and Daining Fang. Multi-scale design of electromagnetic composite metamaterials for broadband microwave absorption. *Composites Science and Technology*, 162:206–214, 2018.

[28] Kai-Lun Zhang, Jun-Ying Zhang, Zhi-Ling Hou, Song Bi, and Quan-Liang Zhao. Multifunctional broadband microwave absorption of flexible graphene composites. *Carbon*, 141:608–617, 2019.

[29] Flaviana Calignano, Diego Manfredi, Elisa Paola Ambrosio, Sara Biamino, Mariangela Lombardi, Eleonora Atzeni, Alessandro Salmi, Paolo Minetola, Luca Iuliano, and Paolo Fino. Overview on additive manufacturing technologies. *Proceedings of the IEEE*, 105(4):593–612, 2017.

[30] V. Laur, Azar Maalouf, A. Chevalier, and Fabrice Comblet. Three-dimensional printing of honeycomb microwave absorbers: Feasibility and innovative multiscale topologies. *IEEE Transactions on Electromagnetic Compatibility*, PP:1–8, 07 2020.

[31] Jian Ren and Jia Yuan Yin. 3d-printed low-cost dielectric-resonator-based ultra-broadband microwave absorber using carbon-loaded acrylonitrile butadiene styrene polymer. *Materials*, 11:1249, 07 2018.

[32] Ding Zhou, Xiaozhong Huang, and Zuojuan Du. Analysis and design of multilayered broadband radar absorbing metamaterial using the 3-d printing technology-based method. *IEEE Antennas and Wireless Propagation Letters*, 16:133–136, 2017.

[33] Xhoandri Lleshi, Thi Quynh Van Hoang, Brigitte Loiseaux, and Didier Lippens. Design and full characterization of a 3-d-printed hyperbolic pyramidal wideband microwave absorber. *IEEE Antennas and Wireless Propagation Letters*, 20(1):28–32, 2021.

[34] Ting Shi, Lei Jin, Lei Han, Ming-Chun Tang, He-Xiu Xu, and Cheng-Wei Qiu. Dispersion-engineered, broadband, wide-angle, polarization-independent microwave metamaterial absorber. *IEEE Transactions on Antennas and Propagation*, 69(1):229–238, 2021.

[35] Majid Amiri, Farzad Tofigh, Negin Shariati, Justin Lipman, and Mehran Abolhasan. Wide-angle metamaterial absorber with highly insensitive absorption for te and tm modes. *Scientific Reports*, 10(1), 2020.

[36] Jianfei Zhu, Zhaofeng Ma, Wujiong Sun, Fei Ding, Qiong He, Lei Zhou, and Yungui Ma. Ultra-broadband terahertz metamaterial absorber. *Applied Physics Letters*, 105(2):021102, 2014.

[37] Élodie Georget, Redha Abdeddaim, and Pierre Sabouroux. A quasi-universal method to measure the electromagnetic characteristics of usual materials in the microwave range. *Comptes Rendus Physique*, 15(5):448–457, 2014. Electromagnetism / Électromagnétisme.

[38] E. Michielssen, J.-M. Sajer, S. Ranjithan, and R. Mittra. Design of lightweight, broadband microwave absorbers using genetic algorithms. *IEEE Transactions on Microwave Theory and Techniques*, 41(6):1024–1031, 1993.

[39] D. Kern and D. Werner. A genetic algorithm approach to the design of ultra-thin electromagnetic bandgap absorbers. *Microwave and Optical Technology Letters*, 38:61 – 64, 07 2003.

[40] Enes Yigit and Hüseyin Duysak. Determination of optimal layer sequence and thickness for broadband multilayer absorber design using double-stage artificial bee colony algorithm. *IEEE Transactions on Microwave Theory and Techniques*, 67(8):3306– 3317, 2019.

[41] MG Moharam and TK Gaylord. Rigorous coupled-wave analysis of planar-grating diffraction. *JOSA*, 71(7):811–818, 1981.

[42] Lifeng Li. Fourier modal method for crossed anisotropic gratings with arbitrary permittivity and permeability tensors. *J. Opt. A: Pure Appl. Opt*, 5:345–355, 07 2003.

[43] Arya Fallahi and Amin Enayati. Modeling pyramidal absorbers using the fourier modal method and the mode matching technique. *IEEE Transactions on Electromagnetic Compatibility*, 58(3):820–827, 2016.